Tetragonal Distortion of Structural Defects in Cr^{3+} Doped in Several Perovskites Calculated from the EPR and Optical Data: A Complete Energy Matrix Study

Ai-Jie Mao[†] and Xiao-Yu Kuang*[,†,‡]

Institute of Atomic and Molecular Physics, Sichuan University, Chengdu 610065, China, and International Centre for Materials Physics, Academia Sinica, Shenyang 110016, China

Received: February 27, 2008; Revised Manuscript Received: April 20, 2008

This paper describes a novel application of a ligand field model in the study of the local molecular structure of the $(CrF_6)^{3-}$ coordination complex. Based on the ligand field model, the complete energy matrix which contains the electron−electron repulsion interaction, the ligand field interaction, the spin−orbit coupling interaction, and the Zeeman interaction, has been constructed for a d^3 configuration ion in a tetragonal ligand field. In order to study the relation between the EPR, the optical spectra, and the local lattice structures around the centers with tetragonal symmetry in AMF_3 codoped with Cr^{3+} and Li^+ ions, a three-layer-ligand model is proposed. By diagonalizing the complete energy matrix and employing the three-layer-ligand model, the variational ranges of the local structural parameters around the Cr^{3+} ions are determined, respectively. The results show that the local lattice structures around the Cr^{3+} ions in AMF_3 exhibit a compressed distortion, and the magnitude of distorted parameter ΔR_1 of the $Cr^{3+}-V_M$ center is different from that of the $Cr^{3+}-Li^+$ center in AMF_3. The compressed distortion is ascribed to the fact that the radius of the Cr^{3+} ion is smaller than those of M^{2+} (M = Cd, Mg, Zn). Moreover, a linear correlation between the difference in the magnitude of distortion parameterΔR for two different defect centers and the difference in the corresponding values of the zero-field-splitting parameter ΔD are found first.

1. Introduction

Impurities in solid materials have been a subject of widespread interest in recent years, as doped materials can display new properties which are absent in pure compounds.[1,2] Among the impurities, particular attention has been focused on the transition-metal ions.[3] Generally, the transition-metal complex molecules may display various spin ground states, such as high-spin, intermediate-spin, or low-spin states, depending on the relative strength of the ligand field energy and the mean spin-pairing energy. In some special cases, i.e., when the ligand field splitting energy becomes comparable with the mean spin-pairing energy, the spin transition phenomena, such as high-spin ↔ low-spin transition, high-spin ↔ intermediate-spin transition, or intermediate-spin ↔ low-spin transition, can be observed.[4–13] In order to understand the various characteristics of transition-metal complex molecules, a careful theoretical study to establish the interrelation between electronic structure and molecular structure will be important. In our present work, the complete energy matrix has been constructed for a d^3 configuration ion in a tetragonal ligand field. By diagonalizing complete energy matrix and employing the three-layer-ligand model, the local lattice structures of the tetragonal $Cr^{3+}-V_M$ and $Cr^{3+}-Li^+$ centers in AMF_3 (A = Rb, Cs, K; M = Cd, Mg, Zn) have been investigated, respectively.

Perovskite fluorides AMF_3 (A = Rb, Cs, K; M = Cd, Mg, Zn) are the most important fluoride crystals because of application in photoelectric basic materials, because they possess excellent insulator, photoluminescent, ferromagnetic, and piezoelectric properties, and so on.[14–18] Especially with transition-metal ions doped in fluoride crystals, those properties may get distinct progress. Recently, a continuing interest in the study of the related properties of Cr^{3+} doped in perovskite fluorides AMF_3 has been intensified for application as tunable solid-state lasers operating at room temperature.[19,20] For example, the EPR spectra of $AMF_3:Cr^{3+}$ systems, which are very sensitive to local lattice structure distortions, have been measured by Takeuchi et al.[21] and Abdulsabirov et al.,[22] respectively; the optical properties of Cr^{3+} doped in $RbCdF_3$, $KMgF_3$, and $KZnF_3$ have been measured by Villacampa et al.[23] and Altshuler et al.,[24] respectively; the investigation of structural phase transitions for Cr^{3+} in $RbCdF_3$ has been reported by Studzinski et al.[25] Yang[26] has investigated the EPR zero-field splitting of Cr^{3+} ions at a tetragonal site and the Cd^{2+} vacancy in $RbCdF_3:Cr^{3+}$ crystals on the basis of high-order perturbation formulas and the first-layer ligands F^-, and a cation vacancy (V_{Cd}) in the third-layer ligands; the second-layer ligands K^+ and the remaining ligands Cd^{2+} in the third layer are not taken into account. When Cr^{3+} and Li^+ ions are codoped in AMF_3, the Cr^{3+} ions are associated with a cation vacancy (V_M) or a Li^+ ion at the nearest divalent-cation site in the third layer due to charge compensation. Moreover, up to now a theoretical explanation for the differences ΔD ($\Delta D = D(V_M) - D(Li^+)$) has not been made. This may be ascribed to the lack of effective calculation formulas related to the structural data for a d^3 configuration in a tetragonal ligand field. In our present work, a three-layer-ligand model is proposed to consider the charge compensation into the calculation. Based on the three-layer-ligand model, the local lattice structures of the tetragonal $Cr^{3+}-V_M$ and $Cr^{3+}-Li^+$ centers in AMF_3 have been investigated by diagonalizing complete energy matrix for a d^3 configuration ion in a tetragonal ligand field. The results show that the local structures around the Cr^{3+} ions in AMF_3 exhibit a compressed distortion, and the distorted parameter of the $Cr^{3+}-V_M$ center is different from that of the $Cr^{3+}-Li^+$

* Corresponding author. E-mail: scu_kxy@163.com or scu_mij@126.com.
† Sichuan University.
‡ Academia Sinica.

10.1021/jp801709u CCC: $40.75
Published on Web 07/11/2008

center. Moreover, the relation between the distorted differences ΔR and the differences ΔD is discussed.

2. Theoretical Method

2.1. Complete Energy Matrix. The perturbation Hamiltonian for a d^3 configuration Cr^{3+} ion in a ligand field with tetragonal symmetry can be expressed by[27,28]

$$\hat{H} = \hat{H}_{ee} + \hat{H}_{LF} + \hat{H}_{SO} + \hat{H}_{ZE}$$
$$= \sum_{i<j} e^2/r_{i,j} + \sum_i V_i + \zeta \sum_i l_i \cdot s_i + \mu_\beta \sum_i (k\vec{l}_i + g_e \vec{s}_i) \cdot \vec{H} \quad (1)$$

where $\hat{H}_{ee}$, $\hat{H}_{LF}$, $\hat{H}_{SO}$, and $\hat{H}_{ZE}$ are, respectively, the electron−electron repulsion interaction, the ligand field interaction, the spin−orbit coupling interaction, and the Zeeman interaction. ζ is the spin−orbit coupling coefficient, k is the orbit reduction factor, and V_i is the ligand field potential:

$$V_i = \gamma_{00} Z_{00} + \gamma_{20} r_i^2 Z_{20}(\theta_i, \varphi_i) + \gamma_{40} r_i^4 Z_{40}(\theta_i, \varphi_i) + \gamma^c_{44} r_i^4 Z^c_{44}(\theta_i, \varphi_i) + \gamma^s_{44} r_i^4 Z^s_{44}(\theta_i, \varphi_i) \quad (2)$$

r_i, θ_i, and φ_i are the coordinates of the ith electron. According to the Hamiltonian (1), the energy matrix for a d^3 configuration ion is constructed. The matrix elements are the functions of the Racah parameters B and C, the spin−orbit coupling coefficient ζ, and the ligand field parameters which are expressed as follows:[29]

$$B_{20} = \frac{1}{2}\sum_\tau G_2(\tau)(3\cos^2\theta_\tau - 1),$$

$$B_{40} = \frac{1}{8}\sum_\tau G_4(\tau)(35\cos^4\theta_\tau - 30\cos^2\theta_\tau + 3),$$

$$B^c_{44} = \frac{\sqrt{70}}{16}\sum_\tau G_4(\tau)\sin^4\theta_\tau \cos 4\phi_\tau,$$

$$B^s_{44} = i\frac{\sqrt{70}}{16}\sum_\tau G_4(\tau)\sin^4\theta_\tau \cos 4\phi_\tau \quad (3)$$

where

$$G_2(\tau) = -q_\tau e G^2(\tau), \quad G_4(\tau) = -q_\tau e G^4(\tau),$$

$$G^k(\tau) = \int_0^{R_\tau} R_{3d}^2(r) r^2 \frac{r^k}{R_\tau^{k+1}}\,dr + \int_{R_\tau}^{\infty} R_{3d}^2(r) r^2 \frac{R_\tau^k}{r^{k+1}}\,dr \quad (4)$$

According to the van Vleck approximation for $G^k(\tau)$ integral,[30] we have the relations

$$G_2(\tau) = -\frac{eq_\tau\langle r^2\rangle}{R_\tau^3}, \quad G_4(\tau) = -\frac{eq_\tau\langle r^4\rangle}{R_\tau^5} \quad (5)$$

By employing the radial wave function of Cr^{3+} ions in complexes,[31] the values of $\langle r^2\rangle$ and $\langle r^4\rangle$ may be estimated as

$$\langle r^2\rangle = 2.4843 \text{ au}, \quad \langle r^4\rangle = 16.4276 \text{ au} \quad (6)$$

Explicitly, the Zeeman term can be expressed by parallel or perpendicular component to the C_4 axis as follows:

$$H_{ZE}(\|) = \mu_\beta \sum_i (kl_{iz} + g_e s_{iz}) H_z,$$

$$H_{ZE}(\perp) = \mu_\beta \sum_i (kl_{ix} + g_e s_{ix}) H_x \quad (7)$$

By using eq 7, the two complete energy matrices including the parallel and perpendicular components of the Zeeman term for a d^3 configuration ion in a tetragonal ligand field have been constructed.

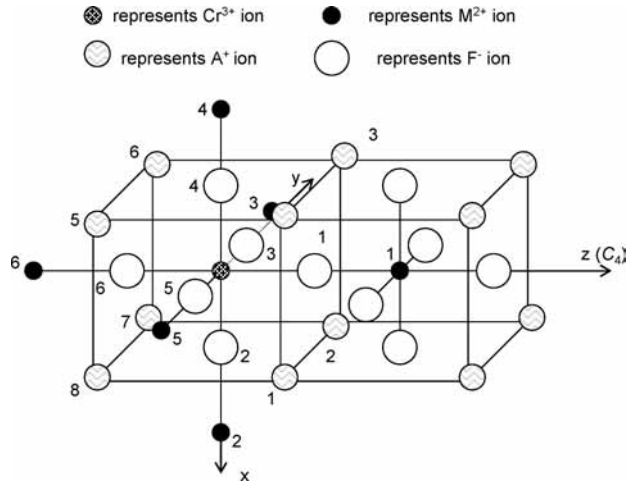

Figure 1. Three-layer-ligand model for the local structure of AMF_3 (A = Rb, Cs, K, M = Cd, Mg, Zn):Cr^{3+} systems.

2.2. ZFS Parameters of a $3d^3$ Ion in a Tetragonal Ligand Field. The EPR spectra of Cr^{3+} ions in a tetragonal ligand field can be described by the spin Hamiltonian:[32]

$$\hat{H}_S = g_\| \mu_\beta H_z S_z + g_\perp \mu_\beta (H_x S_x + H_y S_y) + D[S_z^2 - (1/3)S(S+1)] \quad (8)$$

where D is the zero-field-splitting parameter. From eq 7 the energy levels in the ground state $^4A_2$ without magnetic field are written as follows:

$$E(\pm 1/2) = -D, \quad E(\pm 3/2) = D \quad (9)$$

The corresponding ground-state zero-field splitting ΔE can be expressed as a function of the parameter D:

$$\Delta E = E(\pm 3/2) - E(\pm 1/2) = 2D \quad (10)$$

Based on eqs 3 and 10, the relationship between the local lattice structures of tetragonal $Cr^{3+}-V_M$ and $Cr^{3+}-Li^+$ centers in AMF_3 and its EPR parameters as well as the optical spectra can be investigated by means of the complete energy matrix.

3. Three-Layer-Ligand Model

According to the structural characteristics of AMF_3, the coordinates of the ligands of three-layer-ligand model (as shown in Figure 1) are given in the following. In the first layer, $R_{10}(\tau_1)$ is the bond length of M−F, where $\tau_1 = 1,...,6$ represent the six nearest-neighbor F^- ions. In the second layer, $R_{20}(\tau_2) = \sqrt{3}R_{10}(\tau_1)$ is the bond length of Cr−A (A = K, Rb, Cs), where $\tau_2 = 1,...,8$ denote the eight next-nearest-neighbor A^+ ions. In the third layer, $R_{30}(\tau_3) = 2R_{10}(\tau_1)$ is the bond length of Cr−M (M = Cd, Zn, Mg), where $\tau_3 = 1,...,6$ represent the six next-next-nearest M^{2+} ions. In the calculation we choose the projection of one of the $Cr-F_2$ bonds in the $x-y$ plane along the x-axis (see Figure 2). In this case, the B^s_{44} term is 0 and the angular coordinates of the ligands are given by

$$\theta_{10}(\tau_1)=0,\quad \tau_1=1,\quad \theta_{10}(\tau_1)=\frac{\pi}{2},$$
$$\tau_1=2,3,4,5,\quad \theta_{10}(\tau_1)=\pi,\quad \tau_1=6;$$
$$\phi_{10}(\tau_1)=0,\quad \tau_1=1,2,\quad \phi_{10}(\tau_1)=\frac{\pi}{2},\quad \tau_1=3,$$
$$\phi_{10}(\tau_1)=\pi,\quad \tau_1=4,6,\quad \phi_{10}(\tau_1)=\frac{3}{2}\pi,\quad \tau_1=5;$$
$$\theta_{20}(\tau_2)=\cos^{-1}(1/\sqrt{3}),\quad \tau_2=1,2,3,4,\quad \theta_{20}(\tau_2)=\pi-\cos^{-1}(1/\sqrt{3}),\quad \tau_2=5,6,7,8;$$
$$\phi_{20}(\tau_2)=\frac{\pi}{4},\quad \tau_2=2,7,\quad \phi_{20}(\tau_2)=\frac{3\pi}{4},$$
$$\tau_2=3,6,\quad \phi_{20}(\tau_2)=\frac{5\pi}{4},\quad \tau_2=4,5,\quad \phi_{20}(\tau_2)=\frac{7\pi}{4},$$
$$\tau_2=1,8;\theta_{10}(\tau_3)=0,\quad \tau_3=1,\quad \theta_{10}(\tau_3)=\frac{\pi}{2},$$
$$\tau_3=2,3,4,5,\quad \theta_{10}(\tau_3)=\pi,\quad \tau_3=6;$$
$$\phi_{10}(\tau_3)=0,\quad \tau_3=1,2,\quad \phi_{10}(\tau_3)=\frac{\pi}{2},\quad \tau_3=3,$$
$$\phi_{10}(\tau_3)=\pi,\quad \tau_3=4,6,\quad \phi_{10}(\tau_3)=\frac{3}{2}\pi,\quad \tau_3=5$$

On the basis of the three-layer-ligand model and eq 3, the ligand field parameters can be written as follows:

$$B_{20}=\frac{1}{2}\left[\sum_{\tau_1=1}^{n_1} G_2(\tau_1)(3\cos^2\theta_{\tau_1}-1)+\sum_{\tau_2=1}^{n_2} G_2(\tau_2)\times (3\cos^2\theta_{\tau_2}-1)+\sum_{\tau_3}^{n_3} G_2(\tau_3)(3\cos^2\theta_{\tau_3}-1)\right]$$

$$B_{40}=\frac{1}{8}\left[\sum_{\tau_1=1}^{n_1} G_4(\tau_1)\left(35\cos^4\theta_{\tau_1}-30\cos^2\theta_{\tau_1}+3\right)+\sum_{\tau_2=1}^{n_2} G_4(\tau_2)\left(35\cos^4\theta_{\tau_2}-30\cos^2\theta_{\tau_2}+3\right)+\sum_{\tau_3=1}^{n_3} G_4(\tau_3)(35\cos^4\theta_{\tau_3}-30\cos^2\theta_{\tau_3}+3)\right]$$

$$B_{44}^{c}=\frac{\sqrt{70}}{16}\left[\sum_{\tau_1}^{n_1} G_4(\tau_1)\sin^4\theta_{\tau_1}\cos 4\varphi_{\tau_1}+\sum_{\tau_2}^{n_2} G_4(\tau_2)\sin^4\theta_{\tau_2}\cos 4\varphi_{\tau_2}+\sum_{\tau_3}^{n_3} G_4(\tau_3)\sin^4\theta_{\tau_3}\cos 4\varphi_{\tau_3}\right] \quad (11)$$

where $n_1 = 6$, $n_2 = 8$, and $n_3 = 6$ represent the number of F^- ligands, A^+ ligands, and M^{2+} ligands, respectively.

3.1. M^{2+} Vacancy Model (V_M). The ligand number of the M^{2+} vacancy model is $n_1 = 6$, $n_2 = 8$, and $n_3 = 5$ for six F^- ligands, eight A^+ ligands, and five M^{2+} ligands, respectively. In this case, an M^{2+} vacancy is denoted by $\tau_3 = 1$ along the C_4 axis in the local lattice of the AMF_3:Cr^{3+} system. When Cr^{3+} and Li^+ ions are codoped in AMF_3, Cr^{3+} ions replace M^{2+} ions (M = Cd, Mg, Zn) and the local symmetry around Cr^{3+} ion changes from O_h to C_{4v}. Therefore, we introduce parameters ΔR_1 and ΔR_2 (as shown in Figure 2) to describe the tetragonal distortion in AMF_3. The approximate relationship is used to evaluate the Cr−F bond lengths for Cr^{3+} at the M^{2+} site with C_{4v} symmetry:

$$R_1 = R_{10} - \Delta R_1,\quad R_2 = R_{10} - \Delta R_2 \quad (12)$$

where R_0 is the M−F bond length, and the values are R_{10} = 2.23, 2.20, 2.145, 2.027, and 1.994 Å for $CsCdF_3$, $KCdF_3$, $RbCdF_3$, $KZnF_3$, and $KMgF_3$,[21] respectively. As for the first layer, $A_2 = -eq_\tau\langle r^2\rangle$, $A_4 = -eq_\tau\langle r^4\rangle$, and $A_2/A_4 = \langle r^2\rangle/\langle r^4\rangle$, the ratio of $\langle r^2\rangle/\langle r^4\rangle = 0.151\,227$ for Cr^{3+} may be obtained from the parametric radial wave function.[31] The value of A_4 for octahedral $(CrF_6)^{3-}$ cluster can be determined from the optical spectra and the Cr−F bond length of the CrF_3 and K_2NaCrF_6 crystals.[33−37] By this way, we derive A_4 = 26.525−28.802 au and A_2 = 4.011−4.356 au for octahedral $(CrF_6)^{3-}$ cluster and we will take them in the following calculation. In the second and third layers, the point charges $|e|$ and $|2e|$ will be employed.

The Racah parameters B and C and cubic field parameters Dq can be obtained from their optical spectra or the optical spectra in a similar system;[24,25] the estimated values are listed in Table 1. In the calculation, the spin−orbit coupling coefficient ζ = 217 cm^{-1} [38] is employed for Cr^{3+} in the $KZnF_3$:Cr^{3+} system. Moreover, the slight adjustment from the typical value of $k = 0.79$[38] has been made in order to obtain the values of the g factors ($g_{\|}$, $g_\perp$). By diagonalizing the complete energy matrix with tetragonal symmetry and employing the above parameters, the optical and EPR spectra of the tetragonal

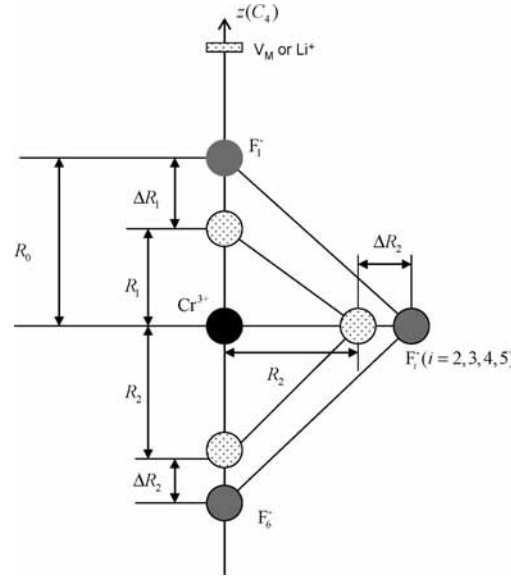

Figure 2. Local structure of the tetragonal $Cr^{3+}-V_M$ and $Cr^{3+}-Li^+$ centers in AMF_3 (A = Rb, Cs, K, M = Cd, Mg, Zn) in the first layer.

TABLE 1: Electrostatic Parameters and Crystal Field Strength Dq of the Tetragonal $Cr^{3+}-V_M$ and $Cr^{3+}-Li^+$ Centers in AMF_3[a]

	B	C	Dq	k	ref
$CsCdF_3$[b]	800	3290	1400	0.77	
$RbCdF_3$	800	3290	1420	0.77	24
$KCdF_3$[b]	745	3315	1525	0.81	
$KZnF_3$	745	3315	1527	0.79	25
$KMgF_3$	742	3330	1560	0.78	25

[a] All values in cm^{-1}. [b] Racah parameters B and C and cubic field parameters Dq for Cr^{3+} doped in $CsCdF_3$ and $KCdF_3$ are estimated from the optical spectra in similar $RbCdF_3$:Cr^{3+} and $KZnF_3$:Cr^{3+} systems, respectively.

TABLE 2: Zero-Field-Splitting Parameters *D* and *g* Factors for $Cr^{3+}-V_M$ Centers in AMF_3 Crystals as a Function of the Two Parameters $\Delta R_1(V_M)$ and $\Delta R_2(V_M)$[a]

	A_4 (au)	$\Delta R_1(V_M)$	$\Delta R_2(V_M)$	$2D(V_M)$	$g_{\|\|}$	$g_\perp$
$CsCdF_3$	26.525	0.3419	0.2730	−0.125 80	1.9700	1.9715
	28.802	0.3104	0.2405	−0.125 80	1.9700	1.9715
experiment[21]				−0.125 86	1.9699	1.9720
$RbCdF_3$	26.525	0.3099	0.2480	−0.113 92	1.9704	1.9718
	28.802	0.2784	0.2156	−0.113 93	1.9704	1.9718
experiment[21]				−0.113 86	1.9705	1.9726
$KCdF_3$	26.525	0.2805	0.2212	−0.102 29	1.9707	1.9721
	28.802	0.2493	0.1892	−0.102 30	1.9707	1.9721
experiment[21]				−0.102 26	1.9705	1.9723
$KZnF_3$	26.525	0.1645	0.1040	−0.108 47	1.9723	1.9736
	28.802	0.1334	0.0721	−0.108 43	1.9723	1.9736
experiment[21]				−0.108 42	1.9720	1.9742
$KMgF_3$	26.525	0.1607	0.792	−0.136 57	1.9729	1.9746
	28.802	0.1300	0.0474	−0.136 58	1.9729	1.9746
experiment[23]				−0.136 60	1.9730	1.9730

[a] ΔR_1 and ΔR_2 are in Å; *D* is cm^{-1}.

TABLE 3: Comparison of Optical Spectra between Theoretical and Experimental Values for $Cr^{3+}-V_M$ Centers in AMF_3 Crystals[a]

		transitions $^4A_2\rightarrow$				
	A_4 (au)	^2E	$^2T_1$	$^4T_2$	$^2T_2$	$^4T_1$
$CsCdF_3$		15 494	16 167	14 002	22 794	21 107
	26.525					
		15 619	16 323	14 583	22 929	23 129
		15 493	16 159	14 002	22 797	21 097
	28.802					
		15 620	16 323	14 576	22 931	23 148
$RbCdF_3$		15 503	16 175	14 181	22 831	21 278
	26.525					
		15 623	16 329	14 714	22 959	23 264
		15 501	16 169	14 181	22 834	21 270
	28.802					
		15 624	16 329	14 709	22 961	23 282
experiment[24]		15 550		14 180		21 300
$KCdF_3$		15 287	15 859	15 249	22 766	22 152
	26.525					
		15 398	16 031	15 791	22 856	24 443
		15 286	15 852	15 247	22 769	22 140
	28.802					
		15 399	16 031	15 782	22 858	24 460
$KZnF_3$		15 281	15 816	15 271	22 799	22 153
	26.525					
		15 405	16 033	15 814	22 879	24 667
		15 280	15 808	15 273	22 804	22 145
	28.802					
		15 406	16 033	15 808	22 880	24 687
experiment[25]		15 364	16 124	15 270	22 470	22 220
$KMgF_3$		15 315	15 792	15 599	22 968	22 642
	26.525					
		15 458	16 069	16 306	23 032	25 626
		15 313	15 780	15 599	22 975	22 630
	28.802					
		15 459	16 069	16 294	23 034	25 652
experiment[25]		15 360	16 300	15 600	22 730	22 570

[a] All values in cm^{-1}.

TABLE 4: Zero-Field-Splitting Parameters *D* and *g* Factors for $Cr^{3+}-Li^+$ in AMF_3 Crystals as a Function of the Two Parameters $\Delta R_1(Li^+)$ and $\Delta R_2(Li^+)$[a]

	A_4 (au)	$\Delta R_1(Li^+)$	$\Delta R_2(Li^+)$	$2D(Li^+)$	$g_{\|\|}$	$g_\perp$
$CsCdF_3$	26.525	0.3748	0.2730	−0.171 74	1.9700	1.9722
	28.802	0.3438	0.2405	−0.171 71	1.9700	1.9722
experiment[21]				−0.171 76	1.9698	1.9728
$RbCdF_3$	26.525	0.3369	0.2480	−0.148 79	1.9704	1.9723
	28.802	0.3058	0.2156	−0.148 76	1.9704	1.9723
experiment[21]				−0.148 78	1.9702	1.9728
$KCdF_3$	26.525	0.3014	0.2212	−0.124 21	1.9711	1.9728
	28.802	0.2705	0.1892	−0.124 18	1.9711	1.9728
experiment[21]				−0.124 24	1.9711	1.9729
$KZnF_3$	26.525	0.1673	0.1040	−0.101 58	1.9723	1.9736
	28.802	0.1363	0.0721	−0.101 59	1.9723	1.9736
experiment[21]				−0.101 60	1.9723	1.9736
$KMgF_3$	26.525	0.1605	0.0792	−0.125 39	1.9729	1.9746
	28.802	0.1299	0.0475	−0.125 48	1.9729	1.9746
experiment[23]				−0.125 40	1.9730	1.9730

[a] ΔR_1 and ΔR_2 are in Å; *D* is in cm^{-1}.

TABLE 5: Comparison of Optical Spectra between Theoretical and Experimental Values for $Cr^{3+}-Li$ Centers in AMF_3 Crystals[a]

		transitions $^4A_2\rightarrow$				
	A_4 (au)	^2E	$^2T_1$	$^4T_2$	$^2T_2$	$^4T_1$
$CsCdF_3$		15 505	16 214	14 002	22 815	21 392
	26.525					
		15 629	16 328	14 890	22 972	23 489
		15 503	16 204	14 002	22 818	21 378
	28.802					
		15 630	16 328	14 879	22 975	23 518
$RbCdF_3$		15 515	16 232	14 181	22 839	21 527
	26.525					
		15 627	16 332	14 973	22 985	23 475
		15 513	16 224	14 181	22 842	21 514
	28.802					
		15 624	16 332	14 965	22 988	23 502
experiment[24]		15 550		14 180		21 300
$KCdF_3$		15 300	15 938	15 249	22 753	22 385
	26.525					
		15 398	16 032	16 017	22 868	24 490
		15 299	15 923	15 247	22 755	22 369
	28.802					
		15 398	16 032	16 006	22 870	24 515
$KZnF_3$		15 302	15 935	15 271	22 735	22 303
	26.525					
		15 390	16 030	15 890	22 840	24 212
		15 301	15 930	15 273	22 738	22 294
	28.802					
		15 391	16 030	15 885	22 842	24 237
experiment[25]		15 364	16 124	15 270	22 470	22 220
$KMgF_3$		15 337	15 939	15 599	22 882	22 755
	26.525					
		15 441	16 066	16 390	22 990	25 075
		15 335	15 931	15 599	22 886	22 742
	28.802					
		15 442	16 066	16 381	22 992	25 106
experiment[25]		15 360	16 300	15 600	22 730	22 570

[a] All values in cm^{-1}.

$Cr^{3+}-V_M$ centers in AMF_3 are simulated by employing two distortion parameters, $\Delta R_1(V_M)$ and $\Delta R_2(V_M)$, and the results are listed in Tables 2 and 3.

3.2. $Cr^{3+}-Li^+$ Center Model. In the $Cr^{3+}-Li^+$ center model, the ligand number is $n_1 = 6$, $n_2 = 8$, and $n_3 = 6$ for six F^- ligands, eight A^+ ligands, and five M^{2+} ligands and one Li^+ ligand. In this case, a Li^+ ion at the nearest M^{2+} site is denoted by $\tau_3 = 1$ along the C_4 axis in the local lattice of the $AMF_3:Cr^{3+}$ system. Then, in the third layer, the point charge $|e|$ will be employed for the $\tau_3 = 1$ ligand. By employing the same parameters and diagonalizing the complete energy matrix with tetragonal symmetry, the relation between the local lattice structure and the EPR and optical spectra of the tetragonal $Cr^{3+}-Li^+$centers in AMF_3 are simulated by employing two distortion parameters, $\Delta R_1(Li^+)$ and $\Delta R_2(Li^+)$, and the results are listed in Tables 4 and 5.

From Tables 2–5, we can see that the distorted parameters for two different tetragonal $Cr^{3+}-V_M$ and $Cr^{3+}-Li^+$ centers in

TABLE 6: Local Lattice Structures of the Tetragonal $Cr^{3+}-V_M$ and $Cr^{3+}-Li^+$ Centers in AMF_3

compound	centers	R_0 (Å)	R_1 (Å)	R_2 (Å)
$CsCdF_3$	$Cr^{3+}-Li^+$		1.8552−1.8862	1.9570−1.9895
		2.230		
	$Cr^{3+}-V_{Cd}$		1.8881−1.9196	1.9570−1.9895
$RbCdF_3$	$Cr^{3+}-Li^+$		1.8631−1.8942	1.9520−1.9844
		2.200		
	$Cr^{3+}-V_{Cd}$		1.8901−1.9216	1.9520−1.9844
$KCdF_3$	$Cr^{3+}-Li^+$		1.8436−1.8745	1.9238−1.9558
		2.145		
	$Cr^{3+}-V_{Cd}$		1.8645−1.8957	1.9238−1.9558
$KZnF_3$	$Cr^{3+}-Li^+$		1.8597−1.8907	1.9230−1.9549
		2.027		
	$Cr^{3+}-V_{Zn}$		1.8625−1.8936	1.9230−1.9549
$KMgF_3$	$Cr^{3+}-Li^+$		1.8335−1.8641	1.9148−1.9466
		1.994		
	$Cr^{3+}-V_{Mg}$		1.8333−1.8640	1.9148−1.9466

AMF_3 are obtained by simulating the calculated optical and EPR spectra for the experimental results simultaneously. Correspondingly, the local structure parameters can also be determined, which are listed in Table 6. $\Delta R_1(V_M \text{ or } Li^+) > 0$ and $\Delta R_2(V_M \text{ or } Li^+) > 0$ denote that the local lattice structures around Cr^{3+} ions in AMF_3 crystals exhibit a compressed distortion whether it is a $Cr^{3+}-V_M$ center or a $Cr^{3+}-Li^+$ center. This may be due to the fact that the radius of Cr^{3+} ions ($r = 0.63$ Å) is smaller than those of M^{2+} (M = Cd, Mg, Zn; $r = 0.97$, 0.66, and 0.74 Å).[39] Moreover, from Tables 2 and 4, we also find that the magnitude of distorted parameters ΔR_1 of the $Cr^{3+}-V_M$ center is smaller than that of the $Cr^{3+}-Li^+$ center in $CsCdF_3$, $RbCdF_3$, $KCdF_3$, and $KZnF_3$, whereas in $KMgF_3$ and the former is almost equal to the latter. Of course, in order to verify our conclusion further, careful experimental investigations, especially ENDOR experiments, are required.

According to the local structure distortion parameters listed in Tables 2 and 4, we find that the difference ΔD ($\Delta D = D(V_M) - D(Li^+)$) is sensitive to ΔR ($\Delta R = \Delta R_1(V_M) - \Delta R_1(Li^+)$) but is not sensitive to $\Delta R'$ ($\Delta R' = \Delta R_2(V_M) - \Delta R_2(Li^+)$). This means that the contribution of the M^{2+} vacancy or Li^+ ion to D cannot be neglected. Moreover, the plots of the differences ΔD ($\Delta D = D(V_M) - D(Li^+)$) versus the distorted differences ΔR ($\Delta R = \Delta R_1(V_M) - \Delta R_1(Li^+)$) are shown in Figure 3 for $Cr^{3+}-V_M$ and $Cr^{3+}-Li^+$ centers in AMF_3. From Figure 3 we can see that the differences ΔD ($\Delta D = D(V_M) - D(Li^+)$) decrease almost linearly on increasing the distorted differences ΔR ($\Delta R = \Delta R_1(V_M) - \Delta R_1(Li^+)$). That is, a linear correlation between the difference in the magnitude of the distortion parameter ΔR ($\Delta R = \Delta R_1(V_M) - \Delta R_1(Li^+)$)) for two different defect centers and the difference in the corresponding values of the zero-field-splitting parameter ΔD ($\Delta D = D(V_M) - D(Li^+)$) are found.

4. Conclusions

Tetragonal distortion of structural defects in Cr^{3+} doped in several perovskites AMF_3 (A = Rb, Cs, K; M = Cd, Mg, Zn) has been investigated on the basis of the 120 × 120 complete energy matrix containing electron−electron repulsion, ligand field, spin−orbit coupling, and Zeeman interactions for a d^3 configuration ion in a tetragonal ligand field, respectively. When the calculated EPR and optical spectra values are in agreement with the experimental results, the variational ranges of the local structural parameters around the Cr^{3+} ions are determined by diagonalizing complete energy matrix and employing a three-layer-ligand model. The results show that the local lattice by

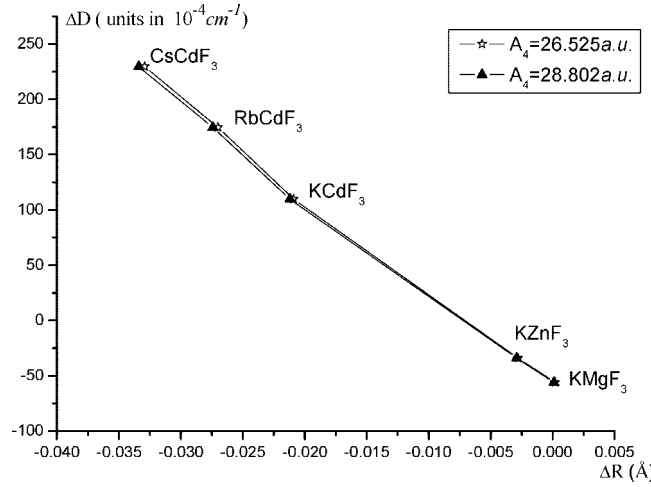

Figure 3. Differences ΔD ($\Delta D = D(V_M) - D(Li^+)$) plotted against distorted differences ΔR ($\Delta R = \Delta R_1(V_M) - \Delta R_1(Li^+)$) for Cr^{3+} and Li^+ ions codoped in AMF_3 (A = Rb, Cs, K, M = Cd, Mg, Zn).

structures around the Cr^{3+} ions in AMF_3 exhibit a compressed distortion, and the magnitude of distorted parameter $\Delta R_1(V_M)$ of the $Cr^{3+}-V_M$ center is different from that of $\Delta R_1(Li^+)$ of the $Cr^{3+}-Li^+$ center in AMF_3. The compressed distortion is ascribed to the fact that the radius of the Cr^{3+} ion is smaller than those of M^{2+} (M = Cd, Mg, Zn). Simultaneously, from our calculation, we can also find that the difference ΔD ($\Delta D = D(V_M) - D(Li^+)$) decreases almost linearly with the increase of the distorted difference ΔR ($\Delta R = \Delta R_1(V_M) - \Delta R_1(Li^+)$).

Acknowledgment. This project was supported by the National Natural Science Foundation of China (Nos. 10774103 and 10374068) and the Doctoral Education fund of Education Ministry of China (No. 20050610011).

Note Added after ASAP Publication. This article posted ASAP on July 11, 2008. Due to a production error the title has been revised along with equation 11 in the Three-Layer-Ligand Model section. The correct version posted on July 16, 2008.

References and Notes

(1) Zhecheva, E.; Stoyanova, R.; Alcańtara, R.; Tirado, J. L. *J. Phys Chem. B* **2003**, *107*, 4290.
(2) Misra, S. K.; Andronenko, S. I. *J. Phys. Chem. B* **2004**, *108*, 9397.
(3) Jeschke, G. *J. Phys. Chem. B* **2000**, *104*, 8382.
(4) Garcia, Y.; Ksenofontov, V.; Campbell, S. J.; Lord, J. S.; Boland, Y.; Gutlich, P. *J. Phys. Chem. B* **2004**, *108*, 17838.
(5) Ohkoshi, S.; Tokoro, H.; Utsunomiya, M.; Mizuno, M.; Abe, M.; Hashimoto, K. *J. Phys. Chem. B* **2002**, *106*, 2423.
(6) Darkhovshii, M. B.; Tchougreeff, A. L. *J. Phys. Chem. A* **2004**, *108*, 6251.
(7) Hibbs, W.; van Koningsbruggen, P. J.; Arif, A. M.; Shum, W. W.; Miller, J. S. *Inorg. Chem.* **2003**, *42*, 5645.
(8) Fujigaya, T.; Jiang, D. L.; Aida, T. *J. Am. Chem. Soc.* **2003**, *125*, 14690.
(9) Letard, J. F.; Capes, L.; Chastanet, G.; Moliner, N.; Letard, S.; Real, J. A. *Chem. Phys. lett.* **1999**, *313*, 115.
(10) Kahn, O.; Martinez, C. J. *Science* **1998**, *279*, 44.
(11) Lemercier, G.; Bousseksou, A.; Seigneuric, S.; Varret, F.; Tuchagues, J. P. *Chem. Phys. Lett.* **1994**, *266*, 289.
(12) Letard, J. F.; Guionneau, P.; Codjovi, E.; Lavastre, O.; Bravic, G.; Chasseau, D.; Kahn, O. *J. Am. Chem. Soc.* **1997**, *119*, 10861.
(13) Krober, J.; Codjóvi, E.; Kahn, O.; Groliere, F.; Jay, C. *J. Am. Chem. Soc.* **1993**, *115*, 9810.
(14) Aramburu, J. A.; Paredes, J. I.; Barriuso, M. T.; Moreno, M. *Phys. Rev. B* **2000**, *61*, 6525.
(15) Kück, S. *Appl. Phys. B: Laser Opt.* **2001**, *72*, 515.
(16) Meijerink, A. *J. Lumin.* **1995**, *55*, 125.
(17) Agnoli, F.; Zhou, W. L. O.; Connor, C. J. *Adv. Mater.* **2001**, *13*, 1679.

(18) Mortier, M.; Wang, Q.; Buzaré, J. Y.; Rousseau, M.; Piriou, B. *Phys. Rev. B* **1997**, *56*, 3022.
(19) Brauch, U.; Durr, U. *Opt. Lett.* **1984**, *9*, 441.
(20) Brauch, U.; Durr, U. *Opt. Commun.* **1984**, *49*, 61.
(21) Takeuchi, H.; Arakawa, M. *J. Phys. Soc. Jpn.* **1984**, *53*, 376.
(22) Abdulsabirov, R. Y.; Larionov, A. L.; Stepanov, V. G.; Lukin, S. N.; Krygin, I. M. In *Magnetic Resonance and Related Phenomena*; Kundla, E.; Lippamaa, E.; Saluvere, T. Eds.; Springer, Berlin, 1979; p 314.
(23) Villacampa, B.; Casas González, J.; Alcalá, R.; Alonso, P. J. *J.Phys.: Condens. Matter* **1991**, *3*, 8281.
(24) Altshuler, N. S.; Larionov, A. L. *Opt. Spectrosc.* **1989**, *66*, 61.
(25) Studzinski, P.; Spaeth, J. M. *Phys. Status. Solidi B* **1986**, *136*, 735.
(26) Yang, Z. Y. *J. Phys.: Condens. Matter* **2000**, *12*, 4091.
(27) Kuang, X. Y. Ph.D. Thesis, Universite de Paris-sud, 1994; p 14.
(28) Kahn, O. *Molecular Magnetism*; VCH Publishers: New York, 1993; p 31.
(29) Newman, D. J.; Urban, W. *Adv. Phys.* **1975**, *24*, 793.
(30) Van Vleck, J. H. *J. Chem. Phys.* **1932**, *1*, 208.
(31) Zhao, M. G.; Xu, J. A.; Bai, G. R.; Xie, H. S. *Phys. Rev B* **1983**, *27*, 1516.
(32) Abragam, A.; Bleaney, B. *Electron Paramagnetic Resonance of Transition Ions*; Oxford University Press: London, 1970.
(33) Knox, K. *Acta Crystallogr.* **1960**, *13*, 507.
(34) Wood, D. L.; Ferguson, J.; Knox, K.; Dillon, J. F., Jr *J. Chem. Phys.* **1963**, *39*, 890.
(35) Ferguson, J.; Guggenheim, H. J.; Wood, D. L. *J. Chem. Phys.* **1971**, *54*, 504.
(36) Babel, D. R.; Haegele, R. *J. Solid State Chem.* **1976**, *18*, 39.
(37) Pueyo, L.; Richardson, J. W. *J. Chem. Phys.* **1977**, *67*, 3583.
(38) Pilla, O.; Galvanetto, E.; Montagna, M.; Viliani, G. *Phys. Rev. B* **1988**, *38*, 3477.
(39) Cao, X. Z.; Song, T. Y.; Wang, X. Q. *Inorganic Chemistry*; High Educational Press: China, 1997; p 130.

JP801709U